JOURNAL OF AIRCRAFT
Vol. 46, No. 1, January–February 2009

Optimization of Propeller Based Propulsion System

Ohad Gur* and Aviv Rosen†
Technion—Israel Institute of Technology, 32000 Haifa, Israel

DOI: 10.2514/1.36055

Propeller design is a complex task that involves a variety of disciplines, such as aerodynamics, structural analysis, and acoustics. A new method of designing an optimal propeller that is based on a multidisciplinary design optimization approach is presented. By combining various analysis tools with an optimization tool, a powerful and flexible design method is obtained. During the design process, three different optimization schemes are used, leading the design to its optimal goal. This new method is applied to the design of a propeller for an ultralight aircraft. Several optional designs for different design goals are presented. The results of the new method are compared with the results of the classic design method based on Betz's condition, which considers only the aerodynamic performance of the propeller. The importance of addressing the characteristics of the entire air vehicle, its aerodynamic characteristics, and its propulsion system (engine, gear box, etc.), rather than only the isolated propeller is emphasized.

Nomenclature

A	=	propeller disk area
a	=	speed of sound
C_{D0}	=	total parasite drag coefficient
C_L, C_D	=	aircraft lift and drag coefficients
$C_{L\max}$	=	aircraft maximum lift coefficient
C_l, C_d	=	two-dimensional lift and drag coefficients
C_{l-i}	=	design lift coefficient of an airfoil
c	=	chord
D	=	drag force
D'	=	drag per unit length of blade
dT, dQ	=	thrust and torque of a disk annulus
E	=	Young's modulus
$(EA)_{(i)}$	=	tension stiffness of element i
$\mathbf{F}$	=	load force vector
FF	=	fuel flow
FF_0	=	reference fuel flow
f_n	=	noise frequency
f	=	function, cost function
$\tilde{f}$	=	penalized cost function
$\mathbf{g}$, $\mathbf{h}$	=	equality and inequality constraint vectors, respectively
H_F	=	flight altitude
i, j	=	indices
K_{C_L}	=	induced drag factor
K_{wake}	=	part of the parasite drag which is influenced by the propeller wake
L	=	lift
L'	=	lift per unit length of blade
M	=	Mach number
$\mathbf{M}$	=	Mach number vector
M_r	=	projection of $\mathbf{M}$ onto $\mathbf{r}_{\text{rel}}$
$M_{x-(i)}$, $M_{y-(i)}$, $M_{z-(i)}$	=	components of resultant cross-sectional moment along an ith element
N	=	number
N_b	=	number of blades
O, H	=	operators
$P_{(i)}$, $V_{y-(i)}$, $V_{z-(i)}$	=	Components of resultant cross-sectional force along an ith element
P_{out}	=	engine output power
p_{ref}	=	reference pressure
$\bar{p}^2$	=	mean square average of sound pressure
R	=	propeller radius
Re	=	Reynolds number
r	=	radial coordinate
$\mathbf{r}_{\text{rel}}$	=	location vector of an observer relative to noise source
r_{rel}	=	magnitude of $\mathbf{r}_{\text{rel}}$
$\hat{\mathbf{r}}_{\text{rel}}$	=	unit vector in the direction of $\mathbf{r}_{\text{rel}}$
S_W	=	wing area
$\text{SPL}_{\text{harmonic}-i}$	=	ith sound pressure level harmonic
$\text{SPLA}_{\text{harmonic}-i}$	=	ith sound pressure level harmonic as heard by a human ear
T	=	thrust
Th	=	throttle condition
$\mathbf{T}_i$	=	rotation matrix
$\mathbf{T}_{ij}$	=	Lighthill stress tensor
t	=	time
t/c	=	thickness ratio
t_C	=	time duration of noise cycle
$\mathbf{x}$	=	vector of design variables
$\tilde{\mathbf{x}}$	=	position vector of a noise source
y_B, z_B	=	Blade's cross-sectional coordinates
$y_{C-(i)}$, $z_{C-(i)}$	=	coordinates of cross-sectional tension center of an ith element
$v_{(i)}$, $w_{(i)}$	=	components of lateral displacement of an ith element
V	=	resultant cross-sectional velocity
$V_{\text{eq-stall}}$	=	equivalent stall airspeed
V_F	=	vehicle airspeed
$V_{\max}$	=	maximum airspeed
$V_{\max 0}$	=	reference maximum airspeed
$\mathbf{v}$	=	velocity vector of a noise source
W	=	weight
w_a, w_t	=	axial and circumferential induced velocity components, respectively
w_1, w_2	=	weighting factors
α	=	angle of attack
β	=	pitch angle
$\Delta_{\text{dBA-dB}}$	=	Difference between $\text{SPL}_{\text{harmonic}-i}$ and $\text{SPLA}_{\text{harmonic}-i}$
Δp	=	pressure variations due to sound wave
$\Delta\mathbf{p}_{ij}$	=	generalized stress tensor

Presented as Paper 1977 at the 4th AIAA Multidisciplinary Design Optimization Specialist Conference, Schaumburg, Illinois, 7–10 April 2008; received 5 December 2007; revision received 18 June 2008; accepted for publication 30 August 2008.

*Researcher, Faculty of Aerospace Engineering; ohadg@aerodyne.technion.ac.il. Member AIAA.

†Professor, Faculty of Aerospace Engineering; rosen@aerodyne.technion.ac.il. Fellow AIAA.

Δp_{thick}, $\Delta p_{\text{loading}}$ = pressure variations due to thickness and loading noise, respectively
δ = Kronecker's delta function
η_P = propeller efficiency
ρ = air density
ρ_0 = standard sea level air density
σ = density ratio
$\sigma_{xx-(i)}$ = axial stress along an ith element
$\sigma_{yy-(i)}$, $\sigma_{zz-(i)}$ = lateral normal stress components along an ith element
$\bar{\sigma}$ = von Mises stress
$\tau_{xy-(i)}$, $\tau_{xz-(i)}$ = cross-sectional shear stress components along an ith element
$\Phi_{(i)}$ = cross-sectional warping function along an ith element
ϕ_i = penalty factors
φ = inflow angle
$\varphi_{(i)}$ = elastic rotation along an ith element
Ψ_0 = volume of a noise source
Ω = propeller rotational speed
Ω_E = engine rotational speed

I. Introduction

ONE of the important elements that determine the performance of an air vehicle is its propulsion system. The propulsion system includes the engine (internal combustion, turbojet, turboshaft, electric, etc.), the energy source (fuel, batteries, etc.), and, in many cases, a propeller. An example of an aerial propeller design is the Wright flyer's propeller, designed by the Wright brothers themselves [1] and showing an impressive efficiency of approximately 80%. A more recent design resulted in the propeller of the Rutan Voyager (the first nonstop, nonrefueled flight around the world) [2].

Today, attention is once more directed toward this very first aeronautical propulsion device: the propeller. This is due to the increased use of unmanned aerial vehicles (UAVs) [3,4], the growing market of general aviation (GA) [4], the increasing interest in ultralight categories, and the growing importance of environmental issues that has led to the development of all-electric, emissionless vehicles [4,5]. The various categories of air vehicles (UAVs, GA, ultralight, etc.) are quite different with regard to configurations, flight conditions, or typical Reynolds and Mach numbers. Nevertheless, the design process of their propellers and the propeller characteristics are quite similar.

The importance of the propulsion system requires a careful design of its various components. In many cases, the propeller is the simplest and cheapest element of a propeller-based propulsion system; yet, its design has an enormous influence on the efficiency of the entire system. Furthermore, in many cases, the configuration of the propulsion system is determined during the early stages of the project, except for the propeller that can be improved, quite easily, during the late stages of the project or even during operation. This makes the propeller design an important element in the process of designing a new air vehicle or upgrading an existing one.

For many years propeller design concentrated mainly on the aerodynamic aspect, while making sure that structural constraints were not violated. Such a design methodology is described by Borst et al. [6–8], in which the various disciplines of propeller design are treated separately in a serial design manner. Borst presented the application of this method to the design of propellers for remotely piloted vehicles [9] and general aviation [10] aircraft. Another example of the traditional approach to propeller design was presented by Larrabee [11]. All these methods are based on the well-known work of Betz from 1919 [12], in which the condition for a maximum efficiency propeller was defined. Betz used a variational approach to define an optimal propeller. After adopting a few assumptions, he found that the vortex sheets in the wake of an optimal propeller move axially backward as rigid screw surfaces. This result was used later on by others, like Goldstein [13], who derived an expression for the velocity induced by such a wake in the case of lightly loaded propellers, and Theodorsen [14], who extended Goldstein's work to include heavily loaded propellers.

Betz defined the criteria for the maximum efficiency of a propeller under certain operating conditions (airspeed, V_F, and propeller's rotational speed, Ω). He considered two cases: minimum power for a certain predetermined required thrust, T (best endurance), and maximum thrust for a certain power (maximum speed).

Betz's method is still used quite often for propeller design [15]. Yet, the practical design of optimum propellers is more complicated because of the following reasons:

1) In many cases, the design goal is more complicated than reducing the propeller's power or maximizing its thrust at certain operating conditions. First of all, the designer has to consider the entire air vehicle, including its aerodynamic characteristics (drag polar) and its complete propulsion system (propeller, engine, gearbox, and energy source), instead of just the propeller alone [16,17]. A central issue becomes the tailoring of the engine and the propeller. Thus, to increase endurance, one should require a minimum rate of use of the energy source rather than minimizing the required propeller's power. This requirement is associated with the engine characteristics that are functions of the operating conditions.

Moreover, in many cases, optimal design refers to various operating conditions and various aspects. Thus, for example, a designer may be interested in reducing the fuel flow at loiter, while also increasing the climbing rate at takeoff. In other cases, designers are interested in reducing the noise that is produced by the propulsion system, because of environmental issues or to reduce the vehicle's acoustic signature. Dealing with cost functions that are different from power or thrust is not possible when using classic design methods.

2) Any design is subject to various constraints. These constraints may include performance, integrity of the system (structural constraints), safety issues, maintenance issues, noise regulations, etc. The classic method is not capable of taking these constraints into account during the optimization procedure.

3) The classic method is based on the momentum theory and includes additional assumptions. It does not allow the use of more accurate aerodynamic models.

After computers were introduced as engineering design tools, they were used for numerical optimizations during the design process of various products. Many of the early applications of numerical optimization for the design of propellers replicated the traditional design method of Betz, using a relatively simple aerodynamic model of the propeller [18]. Later investigations used more sophisticated aerodynamic models [19–23]. All those investigations presented minor improvements over the traditional propeller design. As already indicated, the main deficiency of Betz's method is its inability to consider aspects other than aerodynamics. Ashley [24], like others later on, indicated that, although numerical optimization had become a mature tool, its use for a single-discipline design often offers negligible advantages when compared with the design of a discipline expert. The advantages of numerical optimization become evident in the case of multidisciplinary design optimization (MDO) [25].

MDO is a promising approach for the complex design of rotary wings, that is, of propellers, rotors, or wind turbines. Thus, the application of MDO to the design of rotary wings has increased during recent years. Most previous investigations were limited to two disciplines: aerodynamic and structural analyses [26,27], or aerodynamic and acoustic ones [28–33]. Most of those investigations involved a relatively small number of design variables and a limited number of constraints and did not consider the entire propulsion system, namely, the coupled system (propeller, gearbox, engine, and energy source) [16]. In addition, the aforementioned MDO investigations used only a single-scheme optimization rather than a mixed strategy optimization like the current model.

In a recent article, Logan et al. [34] indicated that, in the case of a long endurance electric vehicle, "Development of a more robust propeller analysis and/or design capability for this class of vehicle is clearly needed." The new method, which is described in the present paper, tries to fill this need by combining various analyses into a unified MDO tool that can address almost any propeller design

problem while simultaneously considering all the various aspects. By using different optimization schemes, the new method can handle a high number of design variables and design constraints. The aerodynamic characteristics of the air vehicle, as well as the characteristics of the engine, are integral elements of the new propeller design method. Thus, the new model overcomes the weakness of the aforementioned previous models.

II. Analysis Tools

The analysis tools of propeller design include 1) an aerodynamic model, 2) an acoustic model, and 3) a structural model.

Because the optimization procedure involves a very high number of iterations, the different models should be accurate and efficient. Nevertheless, the level of fidelity of the analysis models has an important influence on the applicability of the design process results. Therefore, the accuracy of the various models has been extensively verified against results of other, more complex analyses, or experimental results, as will be described. Yet, because the design process, especially in the case of very demanding goals, may lead to the operation of the propeller in regions in which the analysis may be less accurate (stall, high Mach numbers, etc.), it is useful in those cases to run a sensitivity analysis to examine the influence of inaccuracies of the analysis on the detailed design.

A. Aerodynamic Model

During this analysis, the distribution of the aerodynamic loads along the propeller blades is calculated. These data are used to obtain the propeller thrust and required power. In addition, the distribution of the aerodynamic loads is used as an input to the structural and acoustic analyses. Consequently, an inaccurate aerodynamic model may result in inaccuracies in all other analyses of the propeller.

Blade-element models are usually much more efficient than other aerodynamic models. This is the reason for choosing the momentum/blade-element model as the aerodynamic model for the present MDO analysis.

A blade-element model is based on the division of each blade into small elements (segments). Each element behaves aerodynamically as a wing in a two-dimensional flow. Figure 1 presents a cross section of a blade element of an unswept blade. Although the current research will be limited to unswept blades, the aerodynamic model can be extended quite easily to include swept blades [35,36]. The cross section is defined by its radial coordinate, r. y_B and z_B are the blade cross-sectional coordinates; y_B is parallel to the plane of rotation. V_F is the vehicle airspeed, whereas Ωr is the circumferential velocity due to the blade rotation at the rotational speed Ω. w_a and w_t are the axial- and circumferential-induced velocity components, respectively. The resultant cross-sectional velocity, V, is the sum of the aforementioned components. φ is the inflow angle. The angle of attack, α, is obtained by subtracting φ from the local pitch angle, β. The cross-sectional resultant velocity also defines the cross-sectional Mach number, M, and the Reynolds number, Re.

The cross-sectional two-dimensional lift and drag coefficients, $C_l(\alpha, M, Re)$ and $C_d(\alpha, M, Re)$, are obtained by using an aerodynamic database, which introduces some advantages. The aerodynamic database can take into account (at least partially) viscosity effects (through Reynolds number) and compressibility effects (through Mach number).

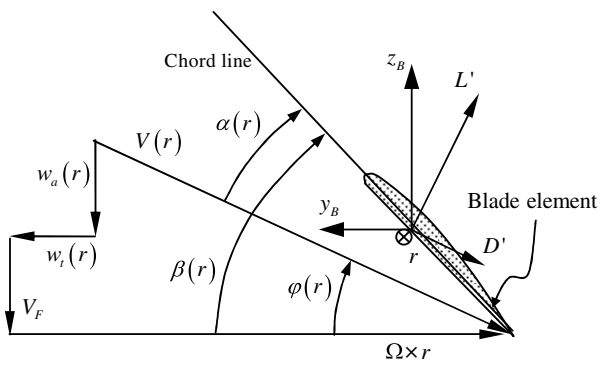

Fig. 1 Cross section of a blade element.

The lift and drag per unit length, L' and D', are

$$L'(r) = \tfrac{1}{2} \cdot \rho \cdot V(r)^2 \cdot c(r) \cdot C_l(\alpha, M, Re) \tag{1}$$

$$D'(r) = \tfrac{1}{2} \cdot \rho \cdot V(r)^2 \cdot c(r) \cdot C_d(\alpha, M, Re) \tag{2}$$

where ρ is the air density and c is the chord of the blade element.

The momentum theory is used to calculate the induced velocity components, w_a and w_t. The propeller is modeled as an actuator disk [37]. The actuator disk is divided into concentric annuli of radius r and width dr. The streamlines passing through the boundaries of each annulus define a set of annular control volumes. According to the momentum theory, the interaction between neighboring control volumes is neglected. Based on this assumption, two equations are obtained for each volume, expressing conservation of axial and rotational momentum [37].

These equations connect the axial and circumferential components of the induced velocity, (w_a, w_t), and the thrust and torque of the disk annulus, (dT, dQ):

$$dT(r) = 4 \cdot \pi \cdot \rho \cdot w_a(r) \cdot [V_F + w_a(r)] \cdot r \cdot dr \tag{3}$$

$$dQ(r) = 2 \cdot \pi \cdot \rho \cdot w_t(r) \cdot r \cdot [V_F + w_a(r)] \cdot r \cdot dr \tag{4}$$

Equations (1) and (2), together with Eq. (3) and (4), are solved for each blade element. Tip effects are introduced into these equations. The resultant force and torque acting on each blade are calculated by integrating the lift and drag that act on each element along the blade.

The regular momentum/blade-element analysis can be extended to include various effects, such as the influence of rotation on the aerodynamic behavior of cross sections in stall [38]. For common operating conditions of propellers, especially those for which the cross sections do not experience stall, the momentum/blade-element model exhibits very good agreement with test results [36].

B. Acoustic Model

The acoustic model is used to calculate the noise that is generated by the propeller, as heard by passengers/crew members in the air vehicle itself or by an observer on the ground.

There may be additional sources of noise apart from the propeller, such as the noise of the turboshaft or internal combustion engine, which can be treated during the design. For an internal combustion engine such as the one that is part of the following examples, an appropriate muffler design can reduce the engine noise significantly. Also, gear boxes produce noise that can be reduced by proper design. The present study will concentrate on propeller noise, which is usually the dominant noise source.

Most of the models that are used to calculate the propeller noise signature are based on the solution of the constrained wave equation, known as the Ffowcs-Williams/Hawkings equation [39]:

$$\frac{1}{a^2} \cdot \frac{\partial^2(\Delta p)}{\partial t^2} - \frac{\partial^2(\Delta p)}{\partial \tilde{x}_i^2} = \frac{\partial^2 T_{ij}}{\partial \tilde{x}_i \cdot \partial \tilde{x}_j} + \frac{\partial}{\partial t}\left\{\rho_a \cdot v_i \cdot \delta(f) \cdot \frac{\partial f}{\partial \tilde{x}_i}\right\} - \nabla\left\{\Delta p_{ij} \cdot \delta(f) \cdot \frac{\partial f}{\partial \tilde{x}_j}\right\} \tag{5}$$

where a is the speed of sound, Δp is the change in the static pressure (relative to the undisturbed pressure), t is time, and $\tilde{\mathbf{x}}$ is the location vector of the noise source relative to a stationary system of coordinates (with components $\tilde{x}_i$). $\mathbf{T}_{ij}$ is the Lighthill stress tensor (with components T_{ij}), $\Delta\mathbf{p}$ is the generalized stress tensor (with components Δp_{ij}), $\mathbf{v}$ is the source velocity vector (with components v_i), and δ is Kronecker's delta function. f is a function that defines the surface of the body that produces the pressure wave (in the present case, it defines the propeller blade):

$$f(\tilde{\mathbf{x}}) = \begin{cases} <0 & \tilde{\mathbf{x}} \text{ inside the body} \\ 0 & \tilde{\mathbf{x}} \text{ on the body surface} \\ >0 & \tilde{\mathbf{x}} \text{ outside the body} \end{cases} \tag{6}$$

The three forcing terms on the right-hand side of Eq. (5), from left to right, represent vortex, thickness, and loading [40]. It was shown that, for thin blades with cross sections operating at subsonic or transonic conditions, the vortex term can be neglected [41]. Thus, the solution of the Ffowcs-Williams/Hawkings equation includes two terms: the thickness noise, Δp_{thick}, and the loading noise, $\Delta p_{\text{loading}}$:

$$\Delta p(\tilde{\mathbf{x}}, t) = \Delta p_{\text{thick}}(\tilde{\mathbf{x}}, t) + \Delta p_{\text{loading}}(\tilde{\mathbf{x}}, t) \tag{7}$$

The solution of the Ffowcs-Williams/Hawkings equation is obtained after applying Green's function [39]. This solution is then discretized [42]. The final expressions for the loading and thickness noise, for a discrete noise source, become

$$\Delta p_{\text{load}}(\tilde{\mathbf{x}}, t) = \frac{1}{4\pi} \cdot \sum_k \left\{ \underbrace{\frac{\dot{\mathbf{F}} \cdot \hat{\mathbf{r}}_{\text{rel}} + \mathbf{F} \cdot \hat{\mathbf{r}}_{\text{rel}} \frac{\dot{\mathbf{M}} \cdot \hat{\mathbf{r}}_{\text{rel}}}{1 - M_r}}{r_{\text{rel}} \cdot a \cdot (1 - M_r)^2}}_{\text{far field}} + \underbrace{\frac{\mathbf{F} \cdot \hat{\mathbf{r}}_{\text{rel}} \frac{1 - \mathbf{M} \cdot \mathbf{M}}{1 - M_r} - \mathbf{F} \cdot \mathbf{M}}{r_{\text{rel}}^2 \cdot (1 - M_r)^2}}_{\text{near field}} \right\} \tag{8}$$

$$\Delta p_{\text{thick}}(\tilde{\mathbf{x}}, t) = \frac{\rho}{4 \cdot \pi} \cdot \sum_k \left\{ \frac{\Psi_0}{r_{\text{rel}} \cdot (1 - M_r)^3} \cdot \left[\frac{\ddot{M}_r}{1 - M_r} + 3\left(\frac{\dot{M}_r}{1 - M_r} \right)^2 + \frac{\dot{M}_r \cdot a \cdot (1 + 2 \cdot M_r)}{r_{\text{rel}} \cdot (1 - M_r)} + 2\left(\frac{M_r \cdot a}{r_{\text{rel}}} \right)^2 \right] \right\}_k \tag{9}$$

The summation sign indicates integration over the entire body. For each element k of the body, $\mathbf{F}$ is the vector of loading force, Ψ_0 is the volume of noise source, $\mathbf{r}_{\text{rel}}$ is location vector of the observer relative to the noise source, $\hat{\mathbf{r}}_{\text{rel}}$ is a unit vector in the direction of $\mathbf{r}_{\text{rel}}$, and r_{rel} is the magnitude of $\mathbf{r}_{\text{rel}}$. $\mathbf{M}$ is a Mach vector, defined as

$$\mathbf{M} = \mathbf{v}/a \tag{10}$$

M_r is the projection of $\mathbf{M}$ onto $\mathbf{r}_{\text{rel}}$ and t is the time as measured in the observer's system, whereas an upper dot indicates a time derivative at the noise source system (measured relative to the retarded time).

Thus, the calculation of the noise that is produced by a propeller is based on dividing the propeller blades into small elements (similar to the aerodynamic blade elements). The pressure disturbance at a certain point in space and at a certain time is calculated after summing up the contributions of all elements according to Eqs. (8) and (9). Then the same process is repeated for the next time step, at which the new positions of the air vehicle and the propeller blades are considered. The pressure wave is defined after repeating this process for a complete cycle (e.g., for a two-bladed propeller, one noise cycle is equivalent to a half-revolution).

The pressure wave undergoes a spectral analysis to find the various sound pressure level harmonics, $\text{SPL}_{\text{harmonic}-i}$, where i is the harmonic number. These harmonics are corrected for the Doppler effect.

In addition, the mean square average of the sound pressure, $\bar{p}^2$, is calculated:

$$\bar{p}^2 = \frac{1}{t_C} \int_0^{t_C} \Delta p^2(\tilde{\mathbf{x}}, t) \tag{11}$$

where t_C is the time duration of a noise cycle.

The mean square average of the sound pressure is used to find the resultant sound pressure level, SPL (given in decibels):

$$\text{SPL} = 10 \times \log_{10} \frac{\bar{p}^2}{p_{\text{ref}}^2} \tag{12}$$

For air, the reference pressure, p_{ref}, is usually chosen as $p_{\text{ref}} = 20 \times 10^{-6}$ Pa.

The noise sensitivity of a human ear depends on the noise frequency, f_n. It is common to define sound harmonics in terms of human ear sensitivity, $\text{SPLA}_{\text{harmonic}-i}$. The differences between $\text{SPL}_{\text{harmonic}-i}$ and $\text{SPLA}_{\text{harmonic}-i}$ are given by an empirical function, $\Delta_{\text{dBA}-\text{dB}}(f_n)$ [43]:

$$\text{SPLA}_{\text{harmonic}-i} = \text{SPL}_{\text{harmonic}-i} + \Delta_{\text{dBA-dB}}(f_n) \tag{13}$$

The total sound pressure level as heard by the human ear, sound pressure level–A weighted (SPLA), is given by the following expression:

$$\text{SPLA} = 10 \times \log_{10}\left[\sum_i \frac{1}{2} \cdot 10^{[\text{SPLA}_{\text{harmonic}-i} - 10 \times \log_{10}(\frac{1}{p_{\text{ref}}^2})]/10} \right] + 10 \times \log_{10}\left(\frac{1}{p_{\text{ref}}^2} \right) \tag{14}$$

Validation of the model by comparison with wind-tunnel and flight test results is presented in [44].

C. Structural Model

Structural analysis is essential to ensure that the propeller blades will be able to withstand the aerodynamic and inertial loads that act along them. A common tool for the structural analysis of blades is finite element modeling [45]. Yet, finite element models require relatively large computer resources and computing time. Thus, for the present case, which requires a very large number of analyses, a more efficient rod model will be used.

The rod structural model describes the propeller blade as a series of straight rod elements located along the blade elastic axis, which is not necessarily a straight line. Thus, curved blades (swept blades) can be used (Fig. 2). The structural cross-sectional properties are uniform along each element and are equal to the structural properties of a representative cross section of that element.

A local Cartesian system of coordinates is attached to each element. $x_{(i)}$ is the coordinate along the ith element, whereas $y_{(i)}$ and $z_{(i)}$ are the cross-sectional coordinates normal to $x_{(i)}$. $\mathbf{T}_{(i)}$ is the rotation matrix between the (i)th and the $(i+1)$th systems of coordinates. The rotation matrix represents the initial curvature and pretwist of the unloaded blade, and the elastic curvature and twist are superimposed on the undeformed geometry. Each element is subject to external loads that include distributed forces and moments. The components of the resultant cross-sectional force along element i are $P_{(i)}$, $V_{y-(i)}$, and $V_{z-(i)}$, whereas the components of the resultant

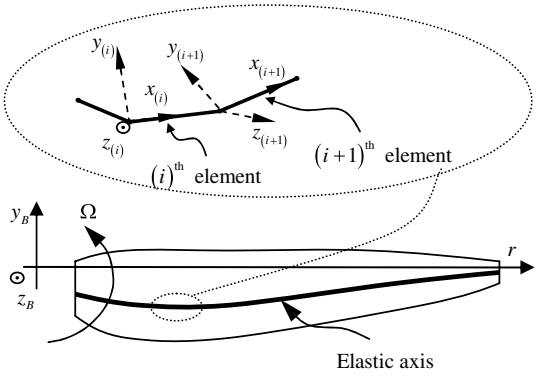

Fig. 2 Structural model.

cross-sectional moment along element i are $M_{x-(i)}$, $M_{y-(i)}$, and $M_{z-(i)}$ in the $x_{(i)}$, $y_{(i)}$, and $z_{(i)}$ directions, respectively.

The deformations along each element are described by the components of the lateral displacement, $(v_{(i)}, w_{(i)})$ in the directions $(x_{(i)}, y_{(i)})$, respectively, and the elastic rotation about the element axis, $\varphi_{(i)}$.

The present analysis will deal with blades made of isotropic material and includes the following two assumptions:

1) Bending analysis is based on the Bernoulli–Euler assumption: sections perpendicular to the elastic axis before deformation remain perpendicular to that axis after deformation.

2) The torsion equation is based on the Saint-Venant assumption: The axial displacement of any cross-sectional point is equal to the product of the cross-sectional warping function, $\Phi_{(i)}(y_{(i)}, z_{(i)})$, and the elastic torsion, $\mathrm{d}\varphi_{(i)}/\mathrm{d}x_{(i)}$.

The structural equations are discretized, leading to a transfer matrix representation [46]. The transfer matrix problem is solved using the boundary condition of a cantilevered rod (clamped root and free tip).

The axial stress, $\sigma_{xx-(i)}$, is [47]

$$\sigma_{xx-(i)}(x_{(i)}, y_{(i)}, z_{(i)}) = E \cdot \left[\frac{P_{(i)}(x_{(i)})}{(EA)_{(i)}} + \frac{d^2 v_{(i)}(x_{(i)})}{dx_{(i)}^2} \cdot [y_{C-(i)} - y_{(i)}] + \frac{d^2 w_{(i)}(x_{(i)})}{dx_{(i)}^2} \cdot [z_{C-(i)} - z_{(i)}] \right] \tag{15}$$

E is the material tension modulus of elasticity (Young's modulus), whereas $(EA)_{(i)}$ is the cross-sectional stiffness in tension. $y_{C-(i)}$ and $z_{C-(i)}$ are the coordinates of the cross-sectional tension center.

The cross-sectional shear stress components, $\tau_{xy-(i)}$ and $\tau_{xz-(i)}$, are calculated based on the components of the cross-sectional resultant shear force, $V_{y-(i)}$ and $V_{z-(i)}$. Then the maximum von Mises stress, $\bar{\sigma}(x_{(i)}, y_{(i)}, z_{(i)})$, at each cross section is calculated [47]:

$$\bar{\sigma}_{(i)}(x_{(i)}, y_{(i)}, z_{(i)}) = \sqrt{[\sigma_{xx-(i)}(x_{(i)}, y_{(i)}, z_{(i)})]^2 + 3 \cdot (\tau_{xy-(i)}^2 + \tau_{xz-(i)}^2 + \tau_{yz-(i)}^2)} \tag{16}$$

As is common in rod models, the contribution of the lateral normal stress components, $\sigma_{yy-(i)}$ and $\sigma_{zz-(i)}$, is neglected.

A detailed description of the model and its validation by comparison with the results of other theoretical models and test results are presented in [48].

III. Propeller Design as an Optimization Problem

A. General Optimization Problem

The propeller design problem is an optimization problem under certain constraints. In general, any optimization problem can be defined as searching for the minimum of a cost function, $f(\mathbf{x})$. $\mathbf{x}$ is the vector of design variables. The design variables are parameters that are controlled by the designer. The cost function represents a measure of the quality of the design. The design is subject to various constraints that include equality constraints, $\mathbf{g}(\mathbf{x})$, and inequality constraints, $\mathbf{h}(\mathbf{x})$.

Thus, a general optimization problem is described as follows:

$$\min_{\mathbf{x} \in \Re^n} [f(\mathbf{x})] \quad \text{subject to } \mathbf{g}(\mathbf{x}) = 0 \quad \mathbf{h}(\mathbf{x}) \leq 0 \tag{17}$$

The penalty method [49] replaces the original problem with an unconstrained optimization problem of a new cost function, $\tilde{f}(\mathbf{x})$:

$$\tilde{f}(\mathbf{x}) = f(\mathbf{x}) + \sum_i \phi_i \cdot O[g_i(\mathbf{x})] + \sum_j \phi_j \cdot H[h_j(\mathbf{x})] \tag{18}$$

ϕ_i is a penalty factor. The operators O and H are defined as follows:

$$O[g_i(\mathbf{x})] = g_i^2(\mathbf{x}) \qquad H[h_i(\mathbf{x})] = \begin{cases} 0 & h_i(\mathbf{x}) \leq 0 \\ h_i^2(\mathbf{x}) & h_i(\mathbf{x}) > 0 \end{cases} \tag{19}$$

B. Propeller Optimization

The present new design method uses the technique of MDO. As already indicated, the analysis tools include three major disciplines: aerodynamics, acoustics, and structural analysis. The ability to simultaneously consider all three disciplines enables the designer to address a wide variety of design problems.

The current research concentrates on the design of the blades. It is clear that the design also includes the propeller hub and spinner. Yet, the influence of the hub and spinner on the performance of the propeller is relatively small [50–52]; thus, their design can be done after the optimal design of the blades.

The design variables during a traditional design process, which is based on Betz's condition, are the pitch angle distribution, $\beta(r)$, chord distribution, $c(r)$, and thickness ratio distribution, $t/c(r)$, of the blade [15]. The present method is capable of dealing with any combination of design variables. The design variables are divided into three main categories: general design variables, blade design variables, and cross-sectional design variables.

The general design variables affect the global configuration and flight conditions of the propulsion system and may include the following parameters: number of propellers; engine related parameters (such as gear ratio); propeller configuration (pusher/tractor); number of propeller blades, N_b; propeller radius, R; rotational speed, Ω; airspeed, V_F; etc.

The blade design variables are parameters that define the geometry and structure of the blade, namely, the distribution along the blade of the following parameters: pitch angle, $\beta(r)$; chord, $c(r)$; sweep angle; dihedral angle; mass; and structural properties.

The blade cross-sectional design variables define the cross-sectional airfoil geometry. In the following examples, the cross sections will belong to the NACA-16 airfoil family [6–8]; thus, the geometry of each cross section is defined by its thickness ratio, t/c, and design lift coefficient, C_{l-i}. These parameters are functions of the radial coordinate, namely, they vary along the blade.

The present design method can deal with almost any cost function. It is possible to replicate Betz's approach by maximizing the propellers' efficiency. On the other hand, more practical cost functions can be dealt with. Thus, if the purpose is increasing endurance, then the cost function becomes the air vehicle fuel flow or the required power from the vehicle batteries (in the case of an electric propulsion system). Using this cost function takes into consideration not only the propeller characteristics, but also the characteristics of the entire propulsion system. Other cost functions may include the propeller noise signature to avoid its acoustic detection.

As already mentioned, the cost function can address more than one goal. It can represent a combination of the vehicle fuel flow and maximum airspeed, thus enabling the design of a propulsion system that is efficient for endurance while also capable of reaching high airspeeds. The final design in this case will present a certain compromise that is essential for vehicles equipped with a constant pitch propeller.

The constraints of the optimization problem are divided into four categories: aerodynamic, acoustic, structural, and side constraints.

Aerodynamic constraints are applied to cases in which the design is subject to performance requirements. These may include cases in which a cost function is the fuel flow and, in addition, a certain maximum airspeed of the air vehicle is required. This kind of constraint ensures that the new propeller will yield good endurance while also offering a high-enough airspeed if needed.

Another example of applying an aerodynamic constraint is the case in which the design goal is to reduce the noise while imposing a limit on performance degradation.

Acoustic constraints can be applied when using an aerodynamic cost function to ensure that the propeller does not become too noisy while maximizing its performance.

Structural constraints are important in almost any design case. In the traditional design process, which is based on Betz's method, the structural constraints are addressed only after completing the aerodynamic optimization. During the present new design method, structural constraints can be introduced as an integral part of the procedure.

Side constraints may include upper and lower bounds on the design variables. In other cases, they may include smoothing constraints imposed by reducing the absolute value of the second derivative of variables along the blade.

C. Optimization Schemes

Three numerical optimization schemes are used during the present design process: 1) heuristic scheme (simple genetic algorithm, or SGA), 2) enumerative scheme (simplex method), and 3) derivative-based scheme (steepest-descent method).

The SGA [53] is based on a natural selection process, similar to an evolution process that includes three major elements: reproduction, crossover, and mutation. Starting from an initial random population of designs and using a genetic scheme leads to an improved population.

In almost all the practical cases, the cost function has more than one minimum, yet only one of those minima is the global one. Heuristic methods are capable of detecting the region of this global minimum better than other methods. At the same time, heuristic schemes result in a "noisy" search process without focusing on a specific area of interest. This noisy process affects the design. In cases in which the design variables describe a physical distribution of parameters (like a distribution along the blade) that should be relatively smooth, the result of the SGA process yields a "spiky," unsmooth distribution.

The next stage of the optimization scheme includes an enumerative simplex scheme. This scheme is capable of dealing efficiently with a large number of design variables, including smoothing constraints of the distribution of variables along the blade. Thus, the distribution of variables along the blade is smoothed out.

The simplex method is based on Nelder and Mead's [54] method, which is different from the well-known linear programming simplex method. Nelder and Mead used a set of $(N+1)$ vectors of design variables where N is the dimension of the design variables' vector, $\mathbf{x}$. Thus, for a two-dimensional problem with two design variables ($N=2$), a simplex is represented by the three vertices of a triangle. For each vertex, the cost function value is calculated. Based on these values, a new, improved simplex is defined. While applying the simplex method, it is not necessary to calculate derivatives; thus, this method offers a relatively high efficiency [55].

A derivative-based method is used only during the final stage of the entire search to pinpoint the final design. These methods are very efficient in unimodal cases (in which the cost function has only one minimum) or in the neighborhood of a minimum and are extensively used [49].

Various versions of derivative-based methods, especially those that are based on Newton's algorithm, use the Hessian matrix of the cost function. The present study will apply a steepest-descent model that uses the gradient vector, but does not use the Hessian matrix. The calculation of the gradient vector involves the calculation of the N first derivatives of the cost function (where N is the number of design variables), meaning at least $2 \cdot N$ calculations of the cost function. Obtaining the Hessian matrix involves the calculation of $N \times N$ second derivatives, meaning at least $3 \cdot N^2$ calculations of the cost function. It is obvious that, in cases of a large number of design variables, the calculation of the Hessian matrix requires a very large amount of computer resources; thus, the steepest-descent method becomes a natural choice.

The use of a "mixed scheme strategy" for optimization (starting with SGA, then using simplex, and, finally, applying the steepest-descent method) exploits the various capabilities of each scheme at different stages of the optimization process. This promises a thorough and complete search for the global minimum.

The designer's role is very important during the aforementioned optimization procedure. It is obvious that the definition of the various optimization elements (design variables, cost function, and constraints) are the responsibility of the designer. Another responsibility includes monitoring the optimization procedure, especially the decision to shift between the various optimization methods.

IV. Representative Examples: Optimizing a Propeller for an Ultralight Aircraft

The purpose of the examples is to demonstrate the capabilities and versatility of the new design method.

An ultralight category aircraft is considered. The aerodynamics of the aircraft is represented by a typical drag polar:

$$C_D = C_{D0} + K_{C_L} \cdot C_L^2 \tag{20}$$

where C_D and C_L are the aircraft drag and lift coefficients, respectively. $K_{C_L} = 0.032$, whereas the parasite drag coefficient is $C_{D0} = 0.03$.

The lift at level flight, L, is equal to the vehicle's weight, W. The required thrust, T, is given by the following expression that describes the increase in vehicle drag due to the propeller wake [56]:

$$T = \frac{D}{1 - K_{\text{wake}} \cdot C_{D0} \cdot \frac{S_W}{A}} \tag{21}$$

where D is the vehicle drag without the propeller wake influence. A is the propeller disk area, whereas S_W is the wing area (in the present example $S_W = 10\ \text{m}^2$). K_{wake} represents the relative area of the vehicle, which is influenced by the propeller wake; thus, its maximum value is unity ($K_{\text{wake}} \leq 1$). In the present example, the maximum value ($K_{\text{wake}} = 1$) will be used, representing the maximum influence of the propeller on the drag.

The vehicle weight is $W = 3950$ N, representing the typical weight of an ultralight aircraft with 50% fuel. A typical equivalent stall airspeed for the ultralight category is $V_{\text{eq-stall}} = 18$ m/s.

The engine model represents the typical engine of this class, with an output power, P_{out}, that is described by the following equation:

$$\begin{aligned} P_{\text{out}}(\Omega_E[\text{rpm}], Th[\%], \sigma)[\text{kW}] &= (0.2 \cdot \sigma^2 + \sigma - 0.2) \\ &\cdot \frac{Th}{100\%} \cdot \left(2 - \frac{Th}{100\%}\right) \\ &\cdot \begin{bmatrix} -4.190856E-10 \cdot \Omega_E^4 + 4.569701E-06 \cdot \Omega_E^3 - \\ -1.298983E-02 \cdot \Omega_E^2 + 2.075551E+01 \cdot \Omega_E \end{bmatrix} \end{aligned} \tag{22}$$

where Ω_E is the engine rotational speed, Th is the throttle condition (100% represents a full throttle), and σ is the density ratio:

$$\sigma = \rho / \rho_0 \tag{23}$$

where ρ_0 is the standard sea-level density, namely, $\rho_0 = 1.225\ \text{kg/m}^3$, whereas ρ is the ambient air density.

The engine model presented in Eq. (22) is typical of an internal combustion engine. Different types of reciprocating engines or electric motors [44] can also be modeled and incorporated within the design procedure.

The engine brake specific fuel consumption (BSFC) is defined as

$$\text{BSFC} = FF / P_{\text{out}} \tag{24}$$

where FF is the fuel flow. BSFC is given by the following typical equation:

$$\text{BSFC}\left[\frac{\text{kg/s}}{\text{W}}\right] = \frac{2.5 \times 10^{-7} \cdot (\Omega_E[\text{rpm}])^2 - 0.002 \cdot \Omega_E[\text{rpm}] + 6.5}{10^8} \tag{25}$$

The gear ratio between the rotational speed of the engine and the propeller is constant and equal to

$$\Omega_E/\Omega = 2.5 \tag{26}$$

The engine rotational speed, Ω_E, is not allowed to increase above a certain maximum value:

$$\Omega_E < 6000 \text{ rpm} \tag{27}$$

The propeller radius, R, is taken as $R = 0.75$ m.

In the present example, Ω is a parameter that is defined during the optimization process and is a result of the propeller design and engine characteristics.

Six different optimization cases will be considered, according to the following goals: 1) best endurance propeller at a given airspeed, 2) best endurance propeller at a given airspeed under structural constraints, 3) best endurance propeller at a given airspeed under acoustic constraints, 4) best endurance propeller at a given airspeed under acoustic and structural constraints, 5) maximum airspeed propeller, and 6) combined best endurance propeller at a given airspeed and maximum airspeed propeller.

A. Best Endurance Propeller at a Given Airspeed

The endurance flight conditions are

$$H_F = 1000 \text{ m}, \qquad V_F = 28 \text{ m/s} \tag{28}$$

where H_F is the flight altitude and V_F is the airspeed. For those conditions, the drag of the vehicle at zero thrust condition is $D = 248$ N.

At first, Betz's method [15] is used to find the minimum required power propeller that produces the required thrust according to Eq. (21). As indicated earlier, when using Betz's method the propeller rotational speed is a priori assumed. Thus, to find the best propeller, the calculations are repeated for a range of rotational speeds. For each propeller (designed for a specific rotational speed), the fuel flow is calculated by using Eq. (25). The rotational speed that yields the minimum fuel flow determines the optimal design. This propeller rotates at a rotational speed of $\Omega = 1625$ rpm and its fuel flow is $FF = 0.0002471$ kg/s.

The new design method was also used to design a best endurance propeller at the same airspeed. The cost function in this case is the fuel flow. Figure 3 presents the values of the penalized cost function, $\tilde{f}(\mathbf{x})$, as a function of the iteration number, first during the SGA process and then during the simplex search. Figure 4 presents the pitch angle, $\beta(r)$, and the normalized chord distribution, $c/R(r)$, along the blade, as obtained by the SGA and simplex processes. The spiky behavior of the distribution along the blade of the design variables, which was obtained at the end of the SGA process, is very evident. To smooth this distribution and make the design a practical one, smoothing constraints are introduced during the simplex search. These smoothing constraints include an upper limit on the second derivative of the design variables with respect to the radial coordinate. Thus, the pitch angle distribution, $\beta(r)$, is subject to the following constraint:

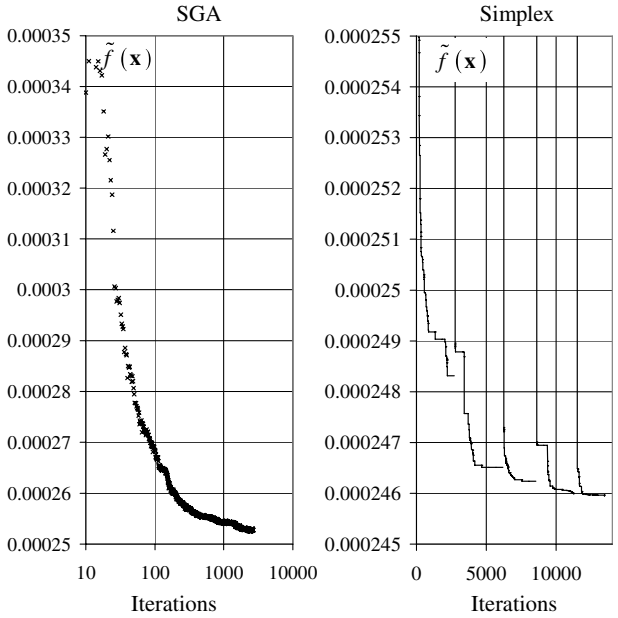

Fig. 3 Penalized cost function during the SGA process and the simplex search.

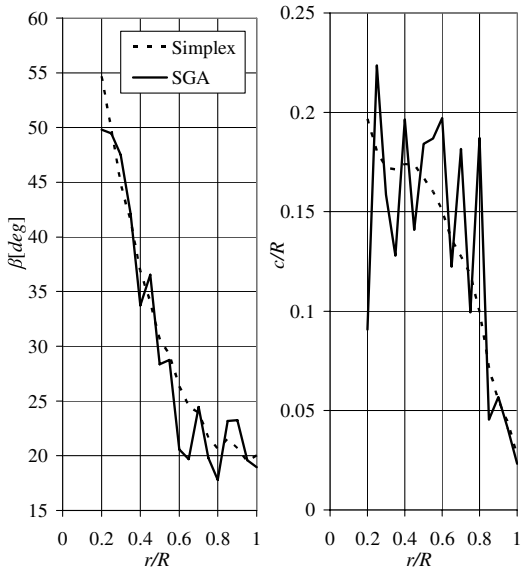

Fig. 4 Comparison of the designs at the end of the SGA process and the simplex search for the best endurance propeller at an airspeed of 28 m/s.

$$\left|\frac{\partial^2 \beta}{\partial r^2}\right| < \text{const.} \tag{29}$$

An effort to include smoothing constraints during the SGA process is very problematic because, as the number of constraints is increased, the SGA process exhibits increasing difficulties in searching for the feasible region. During the simplex search, the smoothing constraints are imposed gradually (namely, the constant value on the right-hand side of Eq. (29) is decreased gradually), resulting in the discontinuous behavior of $\tilde{f}(\mathbf{x})$, as shown in Fig. 3. Figure 4 shows the much-smoother behavior of the results of the simplex process.

A steepest-descent algorithm is used to define the final design, which is shown in Fig. 5 and is compared there with the results of Betz's method. The optimal propeller according to the new design method has a rotational speed of $\Omega = 1643$ rpm and a fuel flow of $FF = 0.0002459$ kg/s. The improvement in the fuel flow, compared with the optimal propeller according to Betz's approach, is very small (0.5%). The pitch distributions exhibit an average difference of 2 deg, with the same general behavior.

The thickness ratio distributions are also shown in Fig. 5. Both methods give similar results, wherein the value, for most of the cross sections, is equal to the lower limit of 0.04. This lower limit is a result of the limited database for the NACA-16 family (which is limited to $t/c \geq 0.04$). Significant differences between the two designs in the value of t/c appear only at the outer 10% of the blade.

The airfoil data include an upper limit of the design lift coefficient: $C_{l-i} \leq 0.7$. When applying Betz's method, the design lift coefficient, C_{l-i}, has been chosen as $C_{l-i} = 0.7$ along the entire blade.

In the case of the normalized chord distribution, c/R, there are certain differences between the results of the present method and Betz's method, especially at the tip.

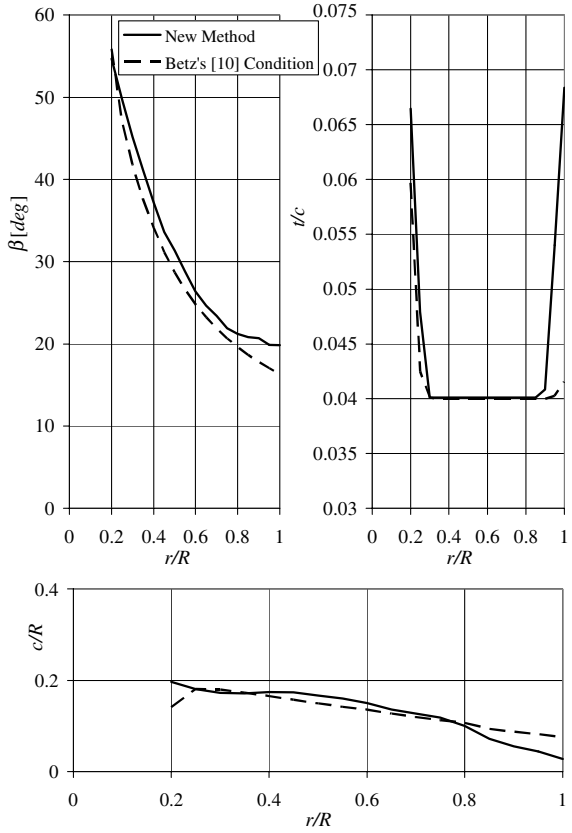

Fig. 5 Design results for a best endurance propeller at an airspeed of 28 m/s.

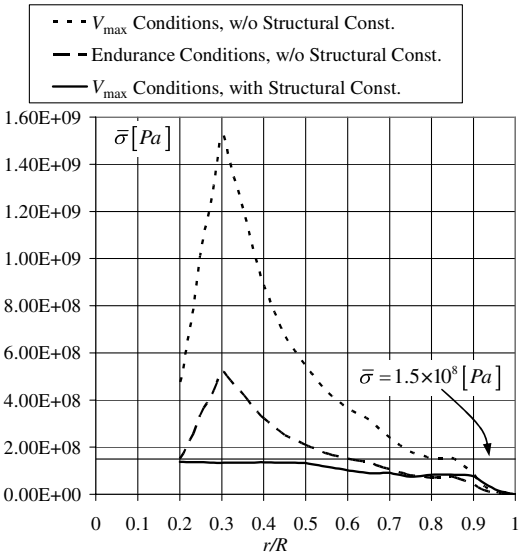

Fig. 6 The maximum cross-sectional von Mises stress distribution along the propellers' blades that were designed in Sec. IV.A, at two flight conditions.

B. Best Endurance Propeller at a Given Airspeed Under Structural Constraints

Figure 6 shows the maximum von Mises stress, $\bar{\sigma}$[Pa], at the cross sections of the optimal blade of the previous subsection. The stress was computed for two flight conditions: 1) endurance conditions as specified in the previous subsection ($H_F = 1000$ m, $V_F = 28$ m/s, and $\Omega = 1643$ rpm), and 2) maximum speed at sea level, $H_F = 0$ ($V_F = 51.2$ m/s and $\Omega = 2400$ rpm).

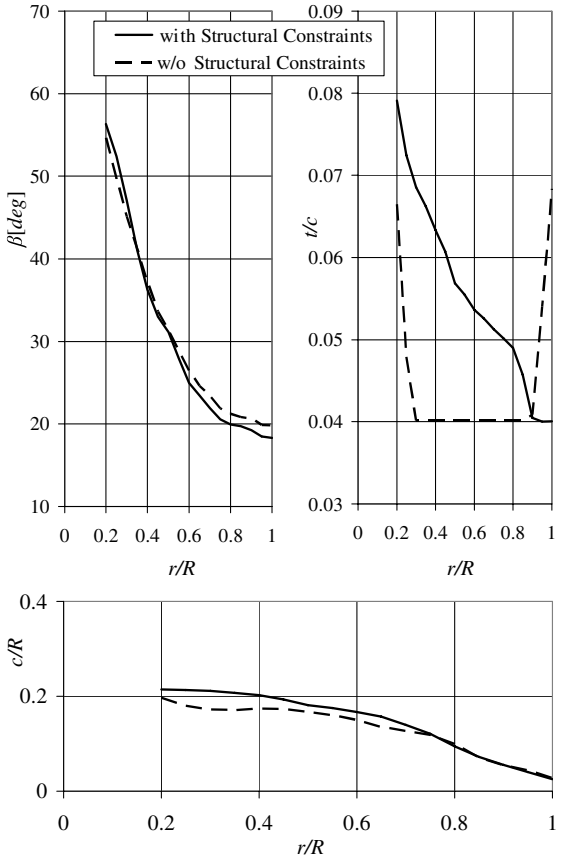

Fig. 7 Design results for the best endurance propeller at an airspeed of 28 m/s including the effect of structural constraints applied at maximum airspeed.

The material of the blade is aluminum 7075-T6. The yield stress for this material is $\sigma_Y = 5.03 \times 10^8$ Pa. The maximum von Mises stress will be limited to

$$\bar{\sigma} < 1.5 \times 10^8 \text{ Pa} \tag{30}$$

The von Mises stresses for this case are presented in Fig. 6 as "w/o Structural Const." curves and are well above the allowed stress along large portions of the blade. This is true for the endurance flight condition and especially true for the condition of maximum airspeed. Thus, a new propeller was designed with the addition of structural constraints, Eq. (30), applied at maximum airspeed.

Figure 7 presents a comparison of the propellers designed with and without structural constraints. The main difference appears in the thickness ratio, t/c, and the normalized chord distribution, c/R. The fuel flow for the propeller designed under structural constraints is $FF = 0.0002480$ kg/s at a rotational speed of $\Omega = 1,653$ rpm.

As indicated in Sec. IV.A, the fuel flow of the propeller that was designed without structural constraints is $FF = 0.0002459$ kg/s at a rotational speed of $\Omega = 1643$ rpm. The increase in the fuel flow as a result of introducing structural constraints is only 0.8%. Figure 6 shows a comparison of the maximum cross-sectional von Mises stress between the propellers designed without and with structural constraints. The stresses for the new design were calculated at the maximum airspeed conditions, which are slightly different for both propellers because of the differences between them: $V_F = 51.2$ m/s and $\Omega = 2400$ rpm for the propeller designed without structural constraints, and $V_F = 50.8$ m/s and $\Omega = 2400$ rpm for the propeller designed with structural constraints. It should be noted that at maximum speed the two designs reach the engine speed limit, Eq. (27). It can be concluded that, at the price of a relatively small degradation in performance (0.8% increase in the fuel flow), the

Table 1 Rotational speed and fuel flow of best endurance propellers designed under different acoustic constraints

Max. SPLA, dBA	Ω, rpm	FF, kg/s	η_P	BSFC, kg/(kW · h)
42.8	1643	0.0002459	0.852	0.0901
40.0	1367	0.0002595	0.832	0.0931
37.5	1167	0.0002890	0.809	0.1006
35.0	994	0.0003324	0.774	0.1107

stresses are reduced significantly to within the allowable range. There is a 1 kg weight penalty associated with the increase in the blade chord and thickness, which is negligible for the present air vehicle.

C. Best Endurance Propeller at a Given Airspeed Under Acoustic Constraints

In the same manner that structural constraints were added to the design of the best endurance propeller in Sec. IV.B, it is possible to add constraints associated with other disciplines. One option is adding acoustic constraints. To demonstrate this option, a constraint on the SPLA, as heard by a stationary observer, is considered. The observer is located at an altitude of 300 m, and the noise is calculated while the vehicle passes right above him or her at a flight altitude of $H_F = 1000$ m (700 m above the observer).

Four cases are compared: the design of best endurance propeller without imposing acoustic constraints (in this case the SPLA is 42.8 dBA) and three other cases in which the noise limits are 40, 37.5, and 35 dBA.

The design of the first case (without any acoustic constraint) was discussed in Sec. IV.A and is presented in Fig. 5. Table 1 presents the rotational speeds and fuel flow of the various propellers. Two trends are clearly observed as the acoustic constraints become more demanding (the allowable SPLA becomes smaller): the rotational speed decreases and the fuel flow increases.

The decrease in the rotational speed is the main mechanism of decreasing the noise signature. The human ear is more sensitive to high frequency noise [43]; thus, as the propeller rotational speed is decreased, the noise signature decreases. The decrease of the rotational speed results in an increase of the cross-sectional pitch angle and chord length to produce the same required thrust. Table 1 presents the propeller efficiency, η_P, and the engine BSFC. As the acoustic constraints become more demanding, the propeller efficiency is decreased while the engine BSFC is increased (resulting in a reduction of 9.2% in the propeller efficiency and an increase of 22.8% in the BSFC, between the extreme cases). These two trends result in a reduction of the entire propulsion system efficiency. This emphasizes the importance of considering the characteristics of the entire propulsion system during the optimization process. Considering only the isolated propeller, without taking into account the engine characteristics, may result in an impractical design.

Figure 8 presents a comparison of the geometry of the various optimal propellers. The increase in the pitch angle and chord, along with the reduction in the propeller's rotational speed, as the acoustic constraints get more demanding is readily noticeable. There are only small differences in the thickness ratio and the design lift coefficient distributions along the blade.

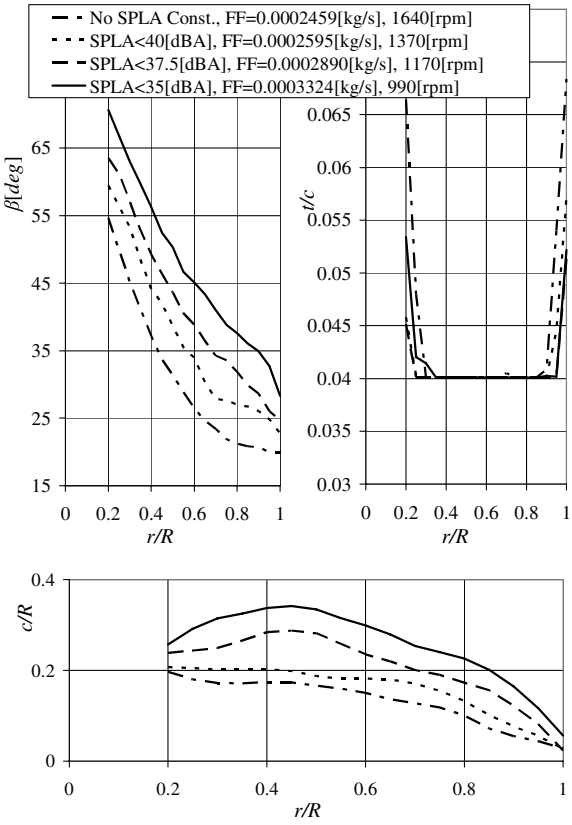

Fig. 8 Geometry of the optimal propeller for the best endurance at an airspeed of 28 m/s under various acoustic constraints.

D. Best Endurance Propeller at a Given Airspeed Under Acoustic and Structural Constraints

In the previous subsections, a design for the best endurance propeller under structural or acoustic constraints was presented. As stated earlier, in practice, structural constraints are part of any design to maintain propeller integrity. Thus, the structural constraints of Sec. IV.B are added to the problem of Sec. IV.C.

The fuel flow, rotational speed, and acoustic signature of the different designs are shown in Table 2. As indicated in Sec. IV.B, the differences in the cost function between the designs with and without stress constraints are negligible. The design trends with and without structural constraints are similar to those presented in Fig. 7; the pitch angle distribution is only slightly influenced by the introduction of structural constraints, whereas the normalized chord and thickness ratio are increased (for more details, see [57]). As presented in Table 2, the differences in design due to the introduction of structural constraints have only a small influence on the fuel flow, propelller efficiency, and engine BSFC.

Table 2 Comparison of optimal endurance propellers with various acoustic and structural constraints

Acoustic const.	Structural constr.	SPLA, dBA	FF, kg/s	Ω, rpm	η_P	BSFC, kg/(kW · h)
W/o	W/o	42.8	0.0002459	1643	0.852	0.0901
W/o	With	43.1	0.0002480	1653	0.845	0.0902
With	W/o	40.0	0.0002595	1367	0.832	0.0931
With	With	40.0	0.0002606	1365	0.830	0.0931
With	W/o	37.5	0.0002890	1167	0.809	0.1006
With	With	37.5	0.0002920	1156	0.805	0.1011
With	W/o	35.0	0.0003324	994	0.774	0.1107
With	With	35.0	0.0003331	992	0.773	0.1108

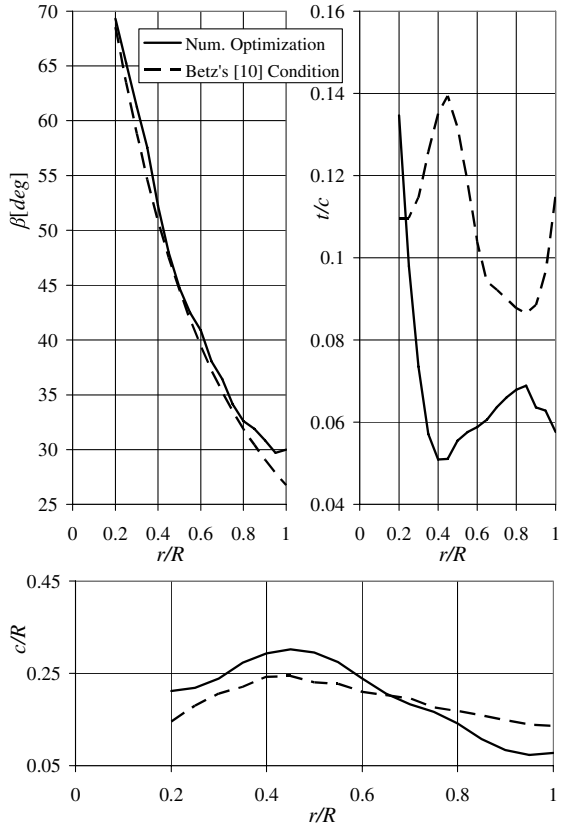

Fig. 9 Comparison of the geometry of the numerical optimization and that obtained by using Betz's condition for the maximum airspeed propeller.

E. Maximum Airspeed Propeller

The aforementioned designs addressed the goal of a maximum endurance propeller at a given airspeed under various constraints. As mentioned earlier, the new design method can cope with cost functions of any kind, including various flight conditions. For the optimal design of a maximum airspeed propeller, the cost function becomes

$$f = 1/V_{\max} \tag{31}$$

where $V_{\max}$ is the airspeed of the aircraft at full throttle or when the engine reaches its upper speed limit.

Betz's method does not address this direct cost function. Instead, it searches for the propeller that produces the maximum thrust for a certain predetermined combination of engine power, propeller rotational speed, and airspeed. This leads to a problem: trying to design the best propeller for maximum airspeed while assuming this airspeed in advance. Thus, the use of Betz's method for the design of a maximum airspeed propeller requires an iterative procedure.

The maximum airspeed flight conditions include sea level altitude ($H_F = 0$) and maximum throttle, with a limit on the engine rotational speed ($\Omega_E < 6000$ rpm, which is equivalent to a propeller rotational speed of $\Omega < 2400$ rpm).

Figure 9 presents a comparison of the design according to Betz's method and the design obtained after using the present new method. The aircraft with the propeller according to Betz's method reaches a maximum airspeed of $V_{\max} = 72.2$ m/s at a rotational speed of $\Omega = 2396$ rpm. The propeller designed by the new method can reach $V_{\max} = 72.5$ m/s at a propeller rotational speed of $\Omega = 2389$ rpm. Similar to the comparison of the designs for best endurance, the difference between the maximum airspeed is very small (0.4%).

The pitch angle distribution of the two propellers (Fig. 9) is similar and reaches an angle of 65 deg at the blade root to cope with the high airspeed. The main difference between the two propellers appears in the chord distribution. The design of the new method has a smaller chord at the tip and a larger chord near the blade hub.

The present design does not include acoustic or structural constraints, which are easy to introduce when using the new method but impossible to impose directly when using Betz's method.

F. Combined Best Endurance Propeller at a Given Airspeed and Maximum Airspeed Propeller

The previous subsections described the design of propellers for two different goals. The first design used fuel flow as the cost function; thus, the goal was best endurance. The second design used $1/V_{\max}$ as the cost function, looking for maximum airspeed. Those two propellers are very different. Table 3 presents a comparison of the two propellers. There is a 24% difference in the fuel flow while flying at the endurance airspeed and a 29% difference in the maximum airspeed.

In many cases the designer is interested in good endurance, namely, low fuel consumption at loiter, while also being able to reach high airspeed if necessary. This implies that the optimal fixed pitch propeller is a compromise between the two aforementioned goals. To express this combined goal, a mixed cost function is defined:

$$f = w_1 \cdot \frac{FF}{FF_0} + w_2 \cdot \frac{V_{\max 0}}{V_{\max}} \tag{32}$$

where w_1 and w_2 are the weighting factors of the two parts in the cost function: the fuel flow part and the maximum airspeed part, respectively. The sum of the two weighting factors is equal to one ($w_1 + w_2 = 1$).

FF_0 is the reference fuel flow, which is the optimum fuel flow when best endurance alone is considered (Sec. IV.A), $FF_0 = 0.0002459$ kg/s. The reference maximum airspeed (Sec. IV.E), $V_{\max 0}$, is the maximum airspeed when a propeller for maximum speed alone is considered, $V_{\max 0} = 72.51$ m/s. Thus, for the cases ($w_1 = 1$ and $w_2 = 0$) or ($w_1 = 0$ and $w_2 = 1$), the cost function will be $f = 1$.

Except for the two boundary cases ($w_1 = 1$, $w_2 = 0$ and $w_1 = 0$, $w_2 = 1$), which were considered in Secs. IV.A and IV.E, respectively, three intermediate cases were also analyzed. Thus, a total of five cases are compared in Table 4.

It is interesting to note that the results are divided into two main groups: cases 1 and 2 represent a group in which the emphasis is on the fuel flow, whereas cases 3–5 represent a group in which the emphasis is on the maximum airspeed. These two groups are also evident when comparing the geometric characteristics of the five designs (Fig. 10). The pitch distribution is similar for cases 3–5, whereas cases 1 and 2 exhibit lower pitch angles. The same behavior is evident when considering the normalized chord: cases 1 and 2 have smaller chord values compared with cases 3–5.

Table 3 Comparison of best endurance and maximum airspeed propellers

	Best endurance propeller	Maximum airspeed propeller
Rotational speed at endurance conditions, rpm	1643	1166
Fuel flow at endurance conditions, kg/s	0.0002459	0.0003044
Maximum airspeed, m/s	51.2	72.51
Rotational speed at maximum airspeed, rpm	2400	2389
Thrust produced at maximum airspeed, N	513	1181

Table 4 Performance comparisons between optimal propellers for various weights of the cost function components

				Maximum airspeed conditions			Endurance conditions		
Case no.	w_1	w_2	f	$V_{\max}$, m/s	$\frac{V_{\max-0}}{V_{\max}}$	Ω_E, rpm	FF, kg/s	$\frac{FF}{FF_0}$	Ω_E, rpm
1	1.00	0.00	1.000	51.2	1.416	6000	0.000246	1.000	4106
2	0.75	0.25	1.075	59.7	1.214	6000	0.000253	1.029	3598
3	0.50	0.50	1.094	72.4	1.001	6000	0.000292	1.188	2918
4	0.25	0.75	1.047	72.5	1.001	6000	0.000292	1.188	2902
5	0.00	1.00	1.000	72.51	1.000	5972	0.000305	1.238	2915

V. Conclusions

A new design method for propellers has been presented and discussed. This method includes three major analysis capabilities: aerodynamics, acoustics, and structural. These analyses are combined into a unified MDO tool for designing propellers and take into account the characteristics of the entire air vehicle, that is, the aerodynamic characteristics (e.g., drag polar) and the propulsion system characteristics, namely, engine characteristics, gear ratio, etc. Although traditional propeller design deals with an isolated propeller, the new design method integrates vehicle aerodynamics and engine characteristics into the design process. This ensures that the propeller design is tailored to the specific vehicle with consideration for the actual design goals.

The use of a mixed optimization strategy that combines three different optimization schemes is beneficial when the design problem includes a high number of design variables and constraints. Numerical investigations indicate that using a single optimization scheme leads in many cases to a design that is not optimal (not a global optimum), because of the weakness of the optimization scheme. A synergy of various optimization schemes takes advantage of the strength of each scheme; thus, it offers a method of arriving at a global optimal design independent of an initial design point.

For a traditional design based on Betz's condition, the propeller efficiency is the sole goal. The advantages of the new method are demonstrated in complex design problems that include multidisciplinary goals and constraints. The new design method allows for the definition of almost any practical cost function. In addition, it can also deal with complex cost functions, leading to an optimal compromise between different goals (e.g., best endurance and maximum airspeed). The examples show that the new design method, unlike classical methods, is capable of designing propellers under various constraints, such as acoustic and structural ones.

Adding structural constraints led to only small reductions of the propeller efficiency, whereas significant reductions of the maximal von Mises stresses were shown along the blade. In the present example, an increase of only 0.8% in the fuel flow is shown, whereas the maximum von Mises stress is reduced by 90%.

The addition of acoustic constraints results in an increase of the fuel flow that depends on the magnitude of allowable noise. The main mechanism of propeller silencing is based on reducing its rotational speed. The price of a 2.5, 5, and 7.5 dBA reduction in propeller noise is an increase in fuel flow by 5, 17, and 35%, respectively. This increase in fuel flow is a result of a decrease in propeller efficiency by 2.5, 5.0, and 9.2%, respectively, and, at the same time, an increase of the engine BSFC by 3.5, 11.5, and 22.9%, respectively. This shows the importance of introducing the engine characteristics into the optimization process. It was shown that the addition of structural constraints in the presence of acoustic constraints results in only a very small increase of the fuel flow.

The consideration of an optimal propeller for maximum airspeed resulted in a design that is quite different from the minimum fuel flow propeller. This design uses 24% more fuel flow in loiter but, at the same time, the maximum airspeed is increased by 29%. The new design method allows for a weighted combination between the maximum airspeed and minimum fuel flow during loiter. These designs represent an optimal compromise and, in the present example, led to two main design groups that differ in their emphasis, that is, maximum airspeed or minimum fuel flow.

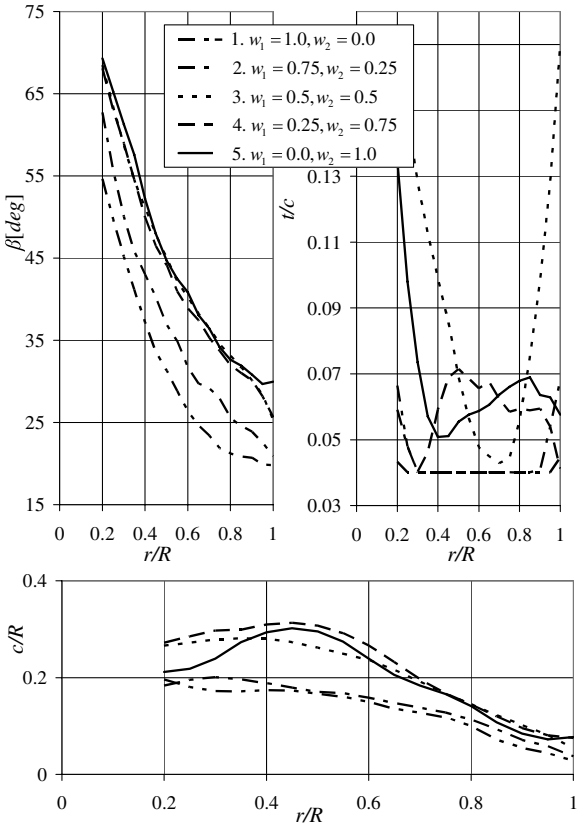

Fig. 10 Comparison of the optimal propellers for various weighting factors of the mixed cost function components.

Acknowledgment

The authors would like to thank Alice Goodman for her thorough reading of the manuscript and useful comments.

References

[1] Wald, Q. R., "The Wright Brothers Propeller Theory and Design," AIAA Paper 2001-3386, July 2001.

[2] Roncz, G. J., "Propeller Development for the Rutan Voyager," Society of Automotive Engineers Paper 891034, April 1989.

[3] Holmes, J. B., Durham, H. M., and Tarry, E. S., "Small Aircraft Transportation System Concept and Technologies," *Journal of Aircraft*, Vol. 41, No. 1, Jan.–Feb. 2004, pp. 26–35.

[4] Carey, B., "Outlook 2007," *Avionics Magazine*, Jan. 2007.

[5] Alexander, D., Lee, Y.-M., Guynn, M., and Bushnell, D., "Emissionless Aircraft Study," AIAA Paper 2002-4056, July 2002.

[6] Borst, H. V., "Summary of Propeller Design Procedures and Data. Volume 1: Aerodynamic Design and Installation," U.S. Army Air Mobility Research and Development Laboratory Technical Report No. 73-34A-VOL-1, Nov. 1973.

[7] Amatt, W., Bates, W. E., and Borst, H. V., "Summary of Propeller Design Procedures and Data. Volume 2: Structural Analysis and Blade Design," U.S. Army Air Mobility Research and Development Laboratory Technical Report No. 73-34B-VOL-2, Nov. 1973.

[8] Sand, E., Elliot, D. A., and Borst, H. V., "Summary of Propeller Design Procedures and Data. Volume 3: Hub, Actuator, and Control Designs ," U.S. Army Air Mobility Research and Development Laboratory Technical Report No. 73-34C-VOL-3, Nov. 1973.
[9] Borst, V. H., "Design and Analysis of Propellers for Low Reynolds Number Application to Mini-RPVs," Society of Automotive Engineers Paper 770999, Feb. 1977.
[10] Borst, V. H., "The Design and Selection of Optimum Propellers for General Aviation Aircraft," Society of Automotive Engineers Paper 790575, Feb. 1979.
[11] Larrabee, E. E., "Practical Design of Minimum Induced Loss Propellers," Society of Automotive Engineers Paper 790585, Feb. 1979.
[12] Betz, A., *Schraubenpropeller mit Geringstem Energieverlust*, Vol. 2, Königliche Gesellschaft der Wissenschaften, Göttingen, Germany, 1919, pp. 193–217; also *Screw Propeller with Minimum Energy Loss*, Technical Translation 736, translated by D. A. Sinclair, National Research Council Library, Canada, 1958.
[13] Goldstein, S., "On the Vortex Theory of Screw Propellers," *Proceedings of the Royal Society of London A*, Vol. 123, No. 792, 1929, pp. 440–465.
[14] Theodorsen, T., *Theory of Propellers*, Publications in Aeronautical Science, McGraw-Hill , New York, 1948, p. 164.
[15] Adkins, C. N., and Liebeck, R. H., "Design of Optimum Propellers," AIAA Paper 83-0190, Jan. 1983.
[16] Monk, J. S., "The Aerodynamic Design of an Optimized Propeller for a High Altitude Long Endurance UAV," *23rd International Congress of Aeronautical Sciences*, International Council of the Aeronautical Sciences, Verneuil-sur-Seine, France, Sept. 2002, pp. 5104.1–5104.9.
[17] Lawrance, A. D., and Mohseni, K., "Efficiency Analysis for Long-Duration Electric MAVs," AIAA Paper 2005-7090, Sept. 2005.
[18] Mendoza, J. P., "Propeller Design by Numerical Optimization," Society of Automotive Engineers Paper 770451, Feb. 1977.
[19] Chang, L. K., and Stefko, G. L., "Application of an Optimization Method to High Performance Propeller Design," AIAA Paper 84-1203, June 1984.
[20] Rizk, M. H., and Jou, W.-H., "Propeller Design by Optimization," AIAA Paper 86-0081, Jan. 1986.
[21] Cho, J., and Lee, S.-C., "Propeller Blade Shape Optimization for Efficiency Improvement," *Computers and Fluids*, Vol. 27, No. 3, March 1998, pp. 407–419.
[22] Ki-Hak, L., Yong-Hee, J., Eui-Sung, B., Dong-Ho, L., and Kyung-Tae, L., "Implementation of the Numerical Optimization for the Micro-Air Vehicle Propeller," AIAA Paper 2004-4428, Sept. 2004.
[23] Burger, C., Hartfield, J. R., and Burkalter, J., "Propeller Performance Optimization Using Vortex Lattice Method and Genetic Algorithm," AIAA Paper 2006-1067, Jan. 2006.
[24] Ashley, H., "On Making Things the Best—Aeronautical Uses of Optimization," *Journal of Aircraft*, Vol. 19, No. 1, Jan. 1982, pp. 5–28.
[25] AIAA Technical Committee on Multidisciplinary Design Optimization, "White Paper on Current State of the Art," Jan. 1991.
[26] Bennet, R. L., "Application of Optimization Methods to Rotor Design Problems," *Vertica*, Vol. 7, No. 3, 1983, pp. 201–208.
[27] Friedmann, P., "Application of Modern Structural Optimization to Vibration Reduction in Rotorcraft," *Vertica*, Vol. 9, No. 4, 1985, pp. 363–376.
[28] Ormsbee, A. I., and Woan, C. J., "Optimum Acoustic Design of Free Running Low Speed Propellers," AIAA Paper 77-1248, Aug. 1977.
[29] Chang, L. K., and Sullivan, J. P., "Optimization of Propeller Blade Shape by an Analytical Method," AIAA Paper 82-1125, June 1982.
[30] Chang, L. K., and Sullivan, J. P., "Optimization of Propeller Blade Twist by an Analytical Method," *AIAA Journal*, Vol. 22, No. 2, Feb. 1984, pp. 252–255.
[31] Miller, J. C., "Optimally Designed Propellers Constrained by Noise," Ph.D. Thesis, Purdue Univ., Dec. 1984.
[32] Miller, J. C., and Sullivan, P. J., "Noise Constraints Effecting Optimal Propeller Designs," *Society of Automotive Engineers, General Aviation Aircraft Meeting and Exposition*, Society of Automotive Engineers, Warrendale, PA, April 1985, pp. 4.585–4.593; also Society of Automotive Engineers Paper 850871.
[33] Drack, E. L., and Wood, A. L., "Design and Analysis of Propellers for General Aviation Aircraft Noise Reduction," International Council of the Aeronautical Sciences Paper 98-5,11,3, Sept. 1998.
[34] Logan, J. M., Chu, J., Motter, A. M., Carter, L. D., Ol, M., and Zeune, C., "Small UAV Research and Evolution in Long Endurance Electric Powered Vehicles," AIAA Paper 2007-2730, May 2007.
[35] Sandak, Y., and Rosen, A., "Aeroelastically Adaptive Propeller Using Blades' Root Flexibility," *The Aeronautical Journal*, Vol. 108, No. 1086, Aug. 2004, pp. 411–418.
[36] Gur, O., and Rosen, A., "Comparison Between Blade-Element Models of Propellers," *48th Israel Annual Conference on Aerospace Sciences*, Technion—Israel institute of Technology, Haifa, Israel, Feb. 2008.
[37] Glauert, H., *Airplane Propellers in Aerodynamic Theory*, Vol. 4, Division L, edited by F. W. Durand, Dover, New York, 1963.
[38] Gur, O., and Rosen, A., "Propeller Performance at Low Advance Ratio," *Journal of Aircraft*, Vol. 42, No. 2, March–April 2005, pp. 435–441.
[39] Ffowcs, J. E. W., and Hawkings, D. L., "Sound Generation by Turbulence and Surfaces in Arbitrary Motion," *Philosophical Transactions of the Royal Society of London*, Vol. 264, No. 1151, 1969, pp. 321–342.
[40] Magliozzi, B., Hanson, D. B., and Amiet, K. R., "Aeroacoustics of Flight Vehicles: Theory and Practice," *Propeller and Propfan Noise* edited by H. H. Hubbard, NASA Reference Publication 1258, Technical Rept. 90-3052, Aug. 1991, Chap. 1.
[41] Hanson, D. B., and Fink, M. R., "The Importance of Quadrupole Sources in Prediction of Transonic Tip Speed Propeller Noise," *Journal of Sound and Vibration*, Vol. 61, No. 1, 1978, pp. 19–38.
[42] Farassat, F., and Succi, G. P., "A Review of Propeller Discrete Frequency Noise Prediction Technology with Emphasis on Two Current Methods for Time Domain Calculations," *Journal of Sound and Vibration*, Vol. 71, No. 3, 1980, pp. 399–419.
[43] Sanford, F., Pearsons, K. S., and Bennett, R. L., "Predicting Aural Detectability of Aircraft in Noise Background," Air Force Flight Dynamics Laboratory TR-72-17, Wright–Patterson Air Force Base, OH, July 1972.
[44] Gur, O., and Rosen, A., "Multidisciplinary Design Optimization of a Quiet Propeller," AIAA Paper 2008-3073, May 2008.
[45] Yamamoto, O., and August, R., "Structural and Aerodynamic Analysis of a Large-Scale Advanced Propeller Blade," *Journal of Propulsion and Power*, Vol. 8, No. 2, March–April, 1992, pp. 367–373.
[46] Leckie, F., and Pestel, E., "Transfer-Matrix Fundamentals," *International Journal of Mechanical Sciences*, Vol. 2, No. 3, 1960, pp. 137–167.doi: 10.1016/0020-7403(60)90001-1
[47] Timoshenko, S., and Goodier, J. N., *Theory of Elasticity*, 2nd ed., McGraw–Hill, New York, 1951, p. 506.
[48] Rosen, A., and Gur, O., "A Transfer Matrix Model of Large Deformations of Curved Rods," *48th Israel Annual Conference on Aerospace Sciences*, Technion—Israel institute of Technology, Haifa, Israel, Feb. 2008.
[49] Boyd, S., and Vandenberghe, L., *Convex Optimization*, Cambridge Univ. Press, New York, 2004, p. 716.
[50] Biermann, D., and Hartman, P. E., "Tests of Five Full-Scale Propellers in the Presence of a Radial and a Liquid-Cooled Engine Nacelle, Including Tests of Two Spinners," NACA TR-642, 1938.
[51] McCormick, B. W., Aljabri, A. S., Jumper, S. J., and Martinovic, Z. N., "The Analysis of Propellers Including Interaction Effects," Society of Automotive Engineers Paper 790576, Feb. 1979.
[52] Borst, V. H., "Propeller Performance and Design as Influenced by the Installation," Society of Automotive Engineers Paper 810602, Feb. 1981.
[53] Goldberg, E. D., *Genetic Algorithms in Search, Optimization, and Machine Learning*, Addison Wesley, Reading, MA, 1989, p. 412.
[54] Nelder, J. A., and Mead, R., "A Simplex Method for Function Minimization," *Computer Journal*, Vol. 7, No. 4, 1965, pp. 308–313.
[55] Van der Velden, A., "Tools for Applied Engineering Optimization," AGARD R803 April 1994.
[56] Biber, K., "Prediction of Propeller Slipstream Drag Count for Turboprop Airplane Performance," AIAA Paper 2005-619, Jan. 2005.
[57] Gur, O., and Rosen, A., "Optimization of Propeller Based Propulsion System," AIAA Paper 2007-1977, April 2008.